ADVANCED ENGINEERING MATERIALS
www.aem-journal.com

# Advanced Plasticized Electroactive Polymers Actuators for Active Optical Applications: Live Mirror

*Kritsadi Thetpraphi, Suphita Chaipo, Waroot Kanlayakan, Pierre-Jean Cottinet, Minh Quyen Le, Lionel Petit, David Audigier, Jeff Kuhn, Gil Moretto, and Jean-Fabien Capsal**

**Herein, an advanced concept to enhance the actuation ability of electroactive polymers (EAPs) based on modified terpolymer P(VDF-TrFE-CFE) is proposed. Such a polymer matrix attracts a great deal of attention because of its outstanding electromechanical coupling property, particularly when doped with plasticizers, e.g., diisononyl phthalate (DINP). Herein, it is demonstrated that by optimizing the structure's multilayer design, the electromechanical coupling of the modified terpolymer is enhanced with its high dielectric permittivity, low Young's modulus, and exceptional dielectric strength. This leads to a large strain response as well as a high mechanical energy density at relatively low electric fields according to the electrostriction phenomena. The concept of stacked multilayers is demonstrated as a simple and effective technique to boost the actuation abilities. Experimental results in accordance with numerical models show actuator performance with a large electromechanical response. This technology shows feasibility for active optical surface shape control. The potential of multiple-stack actuators is tested in a small prototype. This demonstrated mirror optical shape control and correction with a few degrees of freedoms. The proposed Live Mirror technology is useful for ground- and space-based astronomy and communications telescopes.**

The flexibility and semicrystalline structure of electroactive polymers (EAPs) allows a variety of electroactivity developments. The EAPs have been attractive in many sensor–actuator technology fields, especially for electromechanical response[1] in piezoelectric, electrostrictive, and ferroelectric materials. We characterize the response of these polymers to an external electric field with their 1) electrical properties (permittivity, dielectric relaxation, and electrical breakdown) and 2) mechanical properties (Young's modulus).[2] Both characteristics ultimately affect their electromechanical effectiveness. Customized and optimized EAPs have many applications such as rechargeable lithium-ion batteries,[3] enhancing cardiac regeneration,[4] haptic feedback,[5] and tactile sensors.[6] The development of different methods to achieve an excellent actuation response of EAPs was investigated in the polymer/composite,[7] blended polymer,[8] and structural design[9,10] to improve intrinsic properties. Xia et al.[11] introduced a novel relaxor ferroelectric polymer, leading to the future improvement of EAPs for a broader range of electronic applications. Terpolymers P(VDF–TrFE–CFE/CTFE) presenting the combination of the ferroelectric–paraelectric phase yield a high dielectric constant ($\epsilon_r \approx 70$) and large electromechanical reaction. However, the main drawback of these polymers has been their high electric field requirement ($E > 100\,\mathrm{V\,\mu m^{-1}}$)[12] to reach sufficient strain. Hence, the introduction of the terpolymer/composite including an effective fabrication processing/assembly has been investigated to enhance electromechanical effectiveness.[12,13] This motivates the investigation of advanced terpolymer composites by simply adding the plasticizer agent into the terpolymer matrix. The plasticizer molecule leads to the increased molecular mobility of the polymer chains, resulting in an increasing dielectric permittivity and a decrease in the Young's modulus of the material. The charge trapping at the boundaries of the heterogeneous morphology tends to induce large Maxwell–Wagner–Sillars (MWS) polarization effects. Such an adaptation technique is able to exploit electromechanical coupling through areas of functional sensor–actuator fabrication technology.[13]

During the last 10 years, EAPs have been used in several actuator applications, such as artificial muscles,[14] micropumps,[15,16] and smart steerable guidelines.[17] As a result of their flexible and excellent electromechanical properties, EAPs have become attractive soft-actuator candidates in electronic devices. Furthermore, the free-formable attribute of EAPs presents the possibility to carry out numerous different designs. Considering the manufacturing process of piezoelectric and ferroelectric materials for

K. Thetpraphi, S. Chaipo, W. Kanlayakan, Dr. P.-J. Cottinet, Dr. M. Q. Le, Prof. L. Petit, Dr. D. Audigier, Dr. J.-F. Capsal
Univ Lyon, INSA-Lyon, LGEF
EA682, Villeurbanne F-69621, France
E-mail: jean-fabien.capsal@insa-lyon.fr

Dr. G. Moretto
Centre de Recherche Astrophysique de Lyon (CRAL)
9 Avenue Charles André, Saint-Genis-Laval 69230, France

Prof. J. Kuhn
Institute for Astronomy
University of Hawaii
34 Ohia Ku Street, Pukalani, Maui, HI, USA

The ORCID identification number(s) for the author(s) of this article can be found under https://doi.org/10.1002/adem.201901540.

**DOI: 10.1002/adem.201901540**

 

actuator devices, all intermediate processes require many complex components such as the fabrication of lead zirconate titanate by the sol–gel method,[18] the spin-coating process in polyvinylidene fluoride preparation,[19] and monolithic polymer construction.[20] For this reason, to mitigate the complexity of fabrication processes, relaxor ferroelectric polymer (terpolymer) has turned out to be an alternative material in various actuator applications. Apart from intrinsic material modification, there is an opportunity to achieve a large electromechanical response through structure multilayer stacking. For example, 15 layers of terpolymer were used for a microlens application.[21,22] In this article, the modifications of terpolymer characteristics and terpolymer multilayer stacks are explored.

Active optics is a technology used with deformable optical telescopes that are able to maintain telescope optical performance. The active optics technology was developed in the 1980s,[23] when Hardy introduced a new technology of active optics, using cylindrical piezoelectric actuators (Lead Titanate Zirconate) evolving from a separate piston or position actuator to make a small deformable mirror. Freshly, active optics technology is still desirable to overcome technological advancement. Here are some examples of active optic projects-i.e., Observation de la Terre Optique Super-Résolue; high resolution earth observing optical system[24] was designed to have folding mirrors consisted of CILAS 63 actuators piezoelectric monomorph within the controlling system. The Ritchey–Chrétien space telescope[25] was developed and the prototype of an active optics system operated through drive actuators (Piezoknob CLA2201 from Janssen Precision Engineering, JPE). Obviously, the deformable optics control system mostly is involved piezoelectric actuators. Here, we intimated the novelty of implementing EAP actuators in the active optics telescope. The breakthrough targeted by the technology we propose here is to achieve active shape control with many degree-of-freedom force actuators and sensors in an additive 3D printing-based technology that relies on optimized EAP systems. The advantages of free formability (used for local area correction), printability (multishape, multilayer, and massive productivity), and relaxor ferroelectricity (no poling is required and low-driven voltage input is needed) make EAP a promising actuator candidate, applying it in active optics applications.

Recently, our research collaboration introduced a novel hybrid dynamic live optical surface technique,[26–28] which we called the Live Mirror project. Our previous work[29] demonstrated the feasibility of controlling mirror deformation using a single "multilayer plasticized terpolymer" actuator. By inserting an eight-active-layer prestressed actuator between two flat glass plates, a maximum displacement of around 10 μm was attained at a low electric field of 20 V μm$^{-1}$. This technique requires applying compressional stress to the actuator through the glass that induces additional deformation of the glass. Here we show how the symmetric placement of several identical actuators minimizes this effect. This geometry will allow a large-area mirror to be shaped with independent EAP actuator stacks. Experimental measurements together with COMSOL Multiphysics® give a clear understanding on the force generated by the actuator inducing glass deformation with the longitudinal strain 3D color maps at different levels of applied electric fields.

**Figure 1** shows the proposed architecture in the multilayer stack force actuators for "global" shaping (EAP multilayer) and shear electrical polishing (EAP prepolish actuator) modes that should generate, respectively, large longitudinal and transversal strains under moderate electric fields and for realistic load conditions. In the end, a single EAP layer can create shear force-induced glass deformation to give rise to small glass-shape changes. The measurement results together with shear prototype

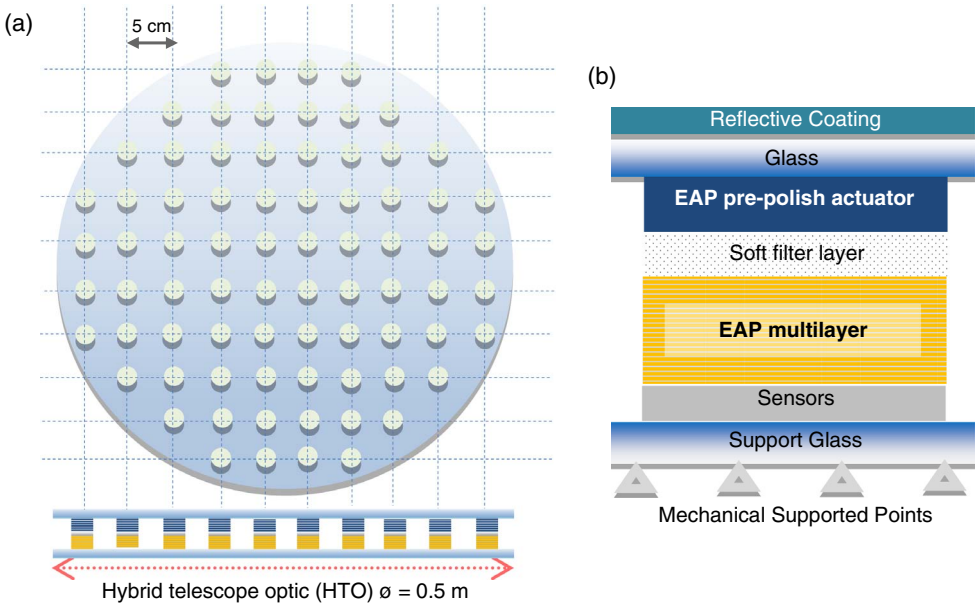


**Figure 1.** a) A design for the hybrid structure of a sandwich of warpable surfaces separated by a lattice of variable force EAP actuators in series with force EAP sensors. b) The shape control system consists of actuator-sensor based EAPs. This particular architecture assumes that shear prepolishing and vertical external force components are controlled by multilayer EAPs.

configuration are demonstrated to show how the shear force generated by actuator expansion can shape the glass surface.

Thin terpolymer films were prepared by the solution blending method. The commercial terpolymer powder (Piezotech S.A.S/Arkema-France) P(VDF-TrFE-CFE) 56.2–36.3–7.5% was dissolved with butanone (methyl ethyl ketone—MEK) in a mass fraction of 20% and mixed with plasticizer agent diisononyl phthalate (DINP). Such a procedure yields a very homogeneous and very smooth thick film between 200 and 250 μm. To achieve the homogenous repartition of external loads applied on the material, a circular shape for the films was optimized and sputtered with 25 nm gold electrodes on both sides.

Regarding several studies on multilayer actuators,[30–32] a functional multilayer topology is designed as a stacking structure and electrically connected in parallel, performing anisotropic *z*-axis electrical conductivity. Such an optimized architecture linearly increases the capacitance of the whole sample proportionally with the number of layers (an eight-layer film including adhesive tape, total thickness is 3 mm).

Concerning actuator performance, four features are relevant to electrostrictive effects on the electroactive polymer. 1) Electrical characterization was presented with the dielectric broadband spectroscopy of dielectric permittivity real part ($\varepsilon'$) and loss tangent ($\tan\delta$) in relation to various frequencies. The measurement was handled throughout sweep frequencies from 50 to 1 MHz at a low applied electric field of 1 $V_{AC}$ at ambient temperature. 2) The mechanical property defined as Young's modulus was characterized at a dynamic stretching of 0.1 Hz alternatively. The tensile specimen size of 1 cm × 4 cm was fixed between a metal holder and a force sensor. 3) The electrical breakdown probability of plasticized films was examined using DC ramp waveform at the rate of 500 V $s^{-1}$. The breakdown measurement setup consists of a wave generator and a high-voltage amplifier. 4) Electromechanical characterization (**Figure 2**) for the modified terpolymer was set up with the above-high-voltage amplifier and waveform generator. The longitudinal strain ($S_{33}$) was measured using a noncontact capacitive sensor with 10 nm precision.

Note that under an excited input voltage, the material deforms itself due to the well-known electrostrictive effect, leading to a variation of the capacitance between the air gap of the sample holder. Such a variation was converted into voltage and the resulting displacement was finally obtained using the sensitivity value of the capacitive sensor (i.e., 0.1 mm $V^{-1}$). The longitudinal strain was deduced by dividing the displacement to initial thickness. Moreover, the multilayer sample leads to a higher precision in displacement measurement than the one-layer sample, thanks to its superior thickness and less flexibility, making it possible to reduce errors from the undesired flexure motion.

The analysis in actuation behavior of the developed material was conducted by evaluating the strain behavior as a function of the applied external load created by different weights. However, actuator performance is not only evaluated by its maximum displacement in free charge but also by its blocking force at very low displacement. Thereby, force measurements define the maximum force generated by the developed EAP (terpolymer) actuator at a given electric field.

The EAP's electrostriction contributes to the quadratic coupling of strain and polarization. In this way, the strain is proportional to a square of the electric field or polarization which can be observed in all materials exhibiting electrostriction.[33]

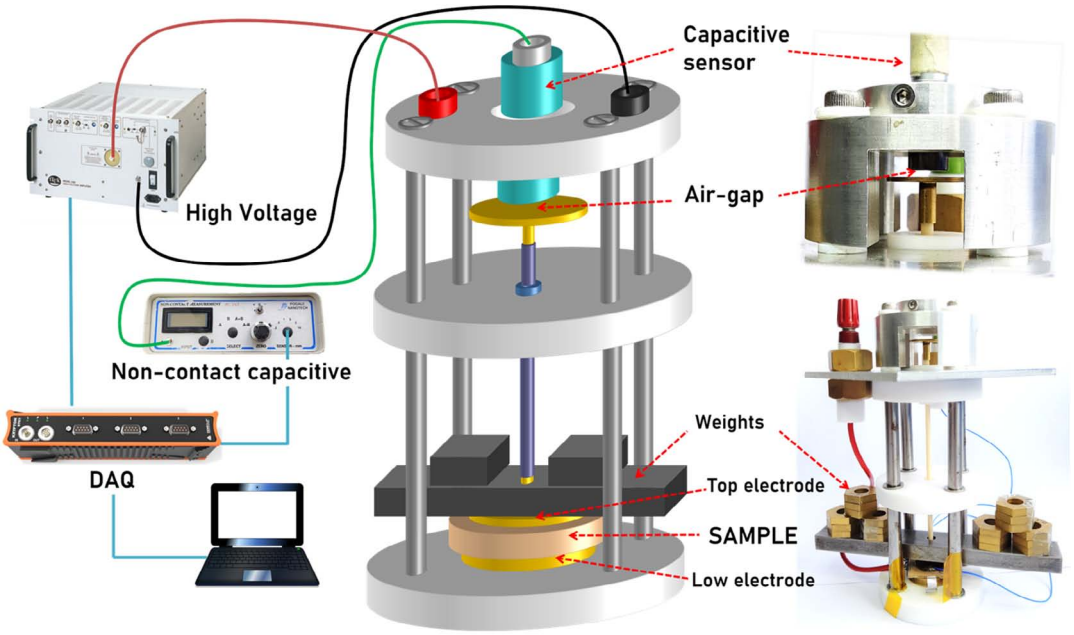


**Figure 2.** The setup for displacement measurement using capacitive displacement sensors to measure the electromechanical activities of the electrostrictive polymer. Avoiding errors in the strain measurements, due the flexure motion mechanical clamping for soft and thin films, samples were on horizontal brass disks. With the aim of creating an electric contact, a second brass disk positioned on top of the film enabled to easily apply an electric field. The whole moving structure included the rod and two discs, having the initial weight of 5 g, which was considered to be a suitable small stress that did not affect the material's movement. To simulate the weight of a piece of glass (Figure 1b), "weights" were successively put on the film.

Induced strain by the external electric field mainly originates from electrostrictive strain ($S_E$), depending on dipole moment interaction within dielectric materials and strain generated by Maxwell stress ($S_M$), resulting from the interaction of free charges between the electrode and/or coulomb interaction.[12] Therefore, the overall strain ($S$) is thus given by

$$S = S_E + S_M = ME^2 \tag{1}$$

where $M$ is the global electrostrictive coefficient and $E$ is an external electric field. Considering the material properties related to the change of strain developed by material polarization, the longitudinal electrostrictive coefficient $M_{33}$ can be defined as

$$M_{33} \propto \frac{\varepsilon_0 \varepsilon_r}{Y} \tag{2}$$

where $\varepsilon_0$ and $\varepsilon_r$ are, respectively, the vacuum and relative permittivity, $Y$ is Young's modulus of the sample. Consequently from Equation (1) and (2), one can see that the strain response can be considerably improved by simultaneously increasing the permittivity and reducing Young's modulus. Several investigations[13,34–36] showed a possibility of achieving this property by doping terpolymer with plasticizers. **Figure 3** shows the analysis of the dielectric constant ($\epsilon_r$) and the loss tangent (tan$\delta$) behavior in the function of various percentages of plasticized terpolymer at sweep frequencies.

As expected, the dielectric constant of the terpolymer significantly enhanced as a function of the DINP content. In such a way the utility of the low molecular weight and the liquid form of the plasticizer agent can serve as the secondary bond inside polymer matrix. This effect tends to increase the free volume and thus the distance between polymer chains, resulting in greater charge mobility for the modified terpolymer with respect to the pure one.[37]

To quantify the dielectric relaxation of the plasticized terpolymer, Figure 3b shows the tan$\delta$ loss broadband spectroscopy, corroborating that the ionic conduction of polymer appears at a low frequency range, and its dissipation factors contain dipolar relaxation losses, ionic conductivity, and interfacial phenomena.[34] Also, the terpolymer with a higher DINP plasticizer content presents the shift of the interfacial relaxation regime toward a higher frequency. Due to the fact that the plasticizer is incorporated into the amorphous phase of the polymer matrix, the agent remains independently without attachment to the primary polymer chain.[37] Both ionic conductivity and interfacial polarization of polymer with a high plasticizer content may take less time to complete polarization on the grounds of its larger amorphous domain and superior charge mobility.[34,37–39] Note that with a dielectric loss at 1 kHz (Figure 3b, small box at top right), the loss tan$\delta$ increased along with the increasing plasticizer fraction—indicating that the loss of energy mostly depends on the defect sector of the blended polymer and ionic conduction at the low frequency range, i.e., DC breakdown strength.

It is established that an exceeded current flow through the dielectric medium may cause electrical breakdown, which limits its energy storage and secure operating voltage. The DC breakdown strength probability of the plasticized terpolymer is analyzed via Weibull probability $P(E)$

$$P(E) = 1 - \exp[-(E/\lambda)]^k \tag{3}$$

where $E$ is the breakdown electric field of each sample, $\lambda$ is a scale parameter portrayed as the breakdown voltage at 63.2% of breakdown probability, and $k$ is data distribution or standard deviation of the experiment. **Figure 4** shows the breakdown probability of the modified (DINPs) plasticized terpolymer compared with the pure one. The dot curve represents the experimental measurement of the breakdown measurement, where the solid line relates to the fitting model based on Equation (3). Excellent coherence between experimental and theoretical results has been achieved, allowing to accurately determine two pertinent parameters, i.e., the data distribution ($k$) and the scale parameter ($\lambda$) corresponding to the breakdown voltage at 63.2%. The result revealed that the terpolymer filled with a maximum DINP weight fraction (i.e. 12%) showed the lowest electrical breakdown strength. As a consequence of some defections in the modified terpolymer, adding more plasticizer content can limit the operating voltage, which will be a frontier of strain production. Confirming one of the goals—for Live Mirror actuators—the new optimized material is more adaptable for low-electrical-input applications.

The mechanical characterization of the samples through the measurements of Young's modulus ($Y$) related to electrostriction (2) is shown in **Figure 5**. Note that $Y$ decreases with increasing

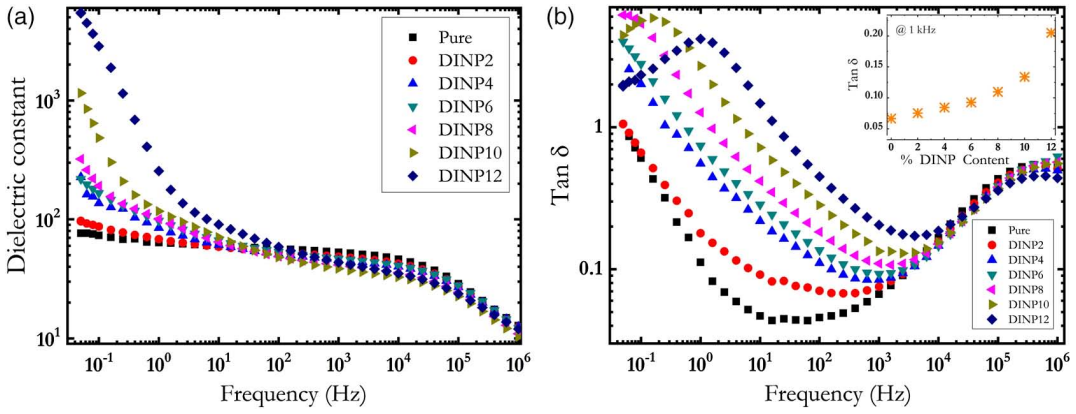


**Figure 3.** Dielectric broadband spectroscopy of terpolymer doped with different DINP contents: a) dielectric permittivity of the real part and b) dissipation factor or loss tangent versus frequency 1 $V_{AC}$.

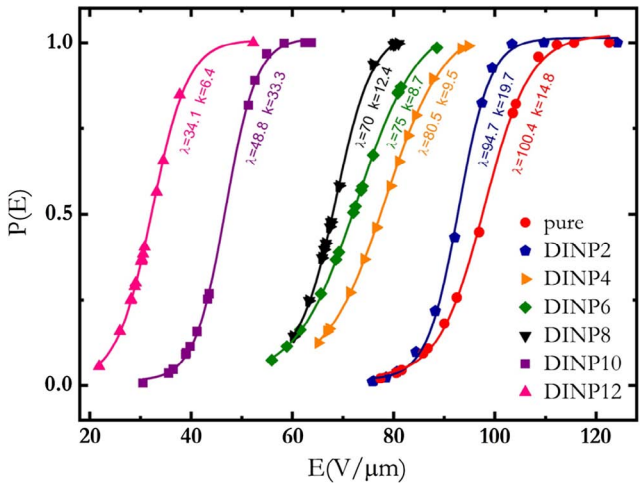


**Figure 4.** Breakdown probability versus electric field of terpolymer/DINP measured with an applied DC ramp.

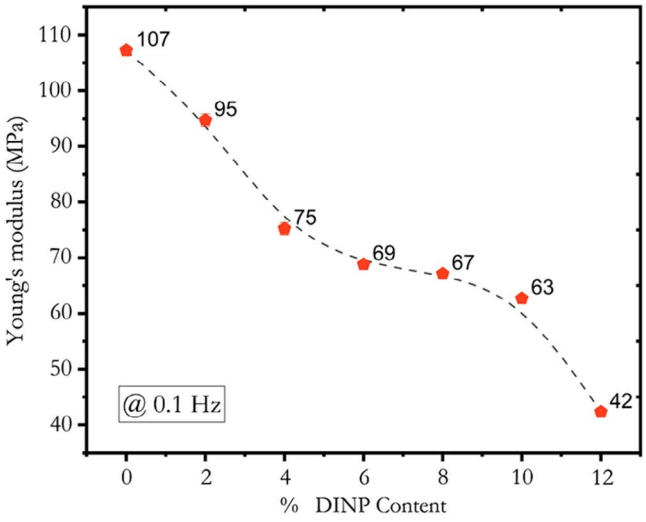


**Figure 5.** Young's modulus of the modified terpolymer with different percentages of the plasticizer at a 0.1 Hz dynamic stretching of 1%.

plasticizer fraction, particularly at 12% (DINP content). As expected, the plasticizer agent was usually used for reducing tensile strength and improving flexibility of the polymer. Notably with DINP, the short chain of phthalate including the polarizable benzene nucleus tends to provide greater flexibility and faster fusion to the polymer matrix with respect to other current industrial plasticizers.[37] In the end, adding DINP agent leads to a reduced Young's modulus and thus the enhanced electromechanical coupling of EAP, but the plasticizer filler quantity should be limited to neither create polymer failure, nor deteriorate dielectric breakdown strength.

One of the key features reflecting actuation performance is related to electromechanical coupling that can be characterized through the conversion between the longitudinal strain ($S_{33}$) and the applied electric field ($E_3$). **Figure 6**a shows the temporal evolution of $S_{33}$ of the modified terpolymer doped with 8% DINP excited by a 50 mHz sinus electric field with 15 V μm$^{-1}$ amplitude. The electrostrictive behavior of the modified sample, with the quadratic dependence of the applied electric field on strain response, is shown in Figure 6b. To optimize the performance of actuation for the multilayer structure, significant load (from 0.76 to 2.74 N) was exerted on the sample at different electric field values (Figure 6c). Such improved results slightly decrease in $S_{33}$, when an extra force was applied to the actuator device.

Despite the fact that the input voltage is limited by the low breakdown strength of the plasticizer agent, the doped terpolymer could achieve a large strain at a very low electric field and significant load conditions.[39] These properties improve the modified materials (plasticized terpolymer) compared with the pure one, where very high voltage is needed to reach the same order of deformation.[34,35] Regarding the dielectric constant ($\varepsilon_r$), terpolymer clearly shows the superior electrostrictive contribution of electromechanical coupling than most classical EAPs. Indeed, the typical dielectric value of conventional EAPs can be found in literature, where $\varepsilon_{r-\mathrm{VHB}} = 4.7$ and $\varepsilon_{r-\mathrm{silicone}} = 3$–4, whereas the one of the terpolymer is much higher, with $\varepsilon_{r-\mathrm{terpolymer}} = 50$. This property makes terpolymer one of the most adequate candidates in the astronomical field, especially in active optics controlling, where a high force is necessary to efficiently deform the mirror surface. Indeed, previous studies[29,35] showed that the figure merit of the blocking force strongly depends on the dielectric permittivity of the material. Based on the analysis investigated in previous work, it has been revealed that the plasticized terpolymer exhibits the largest blocking force as opposed to other former EAPs (i.e. $F_{\mathrm{block\text{-}silicone}} \approx 5$ N, $F_{\mathrm{block\text{-}terpolymer}} \approx 50$ N, and $F_{\mathrm{block\text{-}plasticized\ \ terpolymer}} \approx 200$ N at applied $E = 15$ V μm$^{-1}$).[29] This result allows to confirm high potential of the proposed material in Live Mirror applications. The strain response versus the plasticizer content at a very low electric field (10 V μm$^{-1}$) shows that the actuator ability ultimately depends on an initial load condition and the nature mechanism of the polymer matrix, as shown in Figure 6d.

To compare the permittivity for a pure and modified terpolymer, one should determine the behavior of permittivity in the function of the applied electric field ($E$). An inherent microscopic parameter of dielectric materials induces a polarity in the crystalline phase, allowing to create huge dipole moments in the amorphous regime mainly caused by interfacial phenomena, e.g., MWS polarization. Capsal et al.[36] report the possibility of using Debye/Langevin formalism, predicting the actuation ability of the electrostrictive effect in dielectric materials. Thus, the relative permittivity at a high electric field $\varepsilon'_{(E)}$ is

$$\varepsilon'_{(E)} = 3(\varepsilon_{(E_0 \ll E)} - 1)\left[(E_{\mathrm{SAT}}/E)^2 - \left(1/\sinh^2\left(\frac{E}{E_{\mathrm{SAT}}}\right)\right)\right] \quad (4)$$

where $\varepsilon_{(E_0 \ll E)}$ is the dielectric constant at a very low electric field, $E_{\mathrm{SAT}}$ is the electric field that compensates the temperature depolarization of the dipole, and $E \ll E_{\mathrm{SAT}}$ and $E$ is the local applied electric field. In such a way, Equation (3) enables to evaluate the capacitive current $C_c$ as a function of the applied electric field $E$. The reliability of the current modeled with respect to the experimental current given by the subtraction of leakage current (or conduction current) from the total measured current[40] is shown in **Figure 7**a and the dielectric permittivity at an input electric field up to $E = 20$ V μm$^{-1}$ is shown in Figure 7b. Both

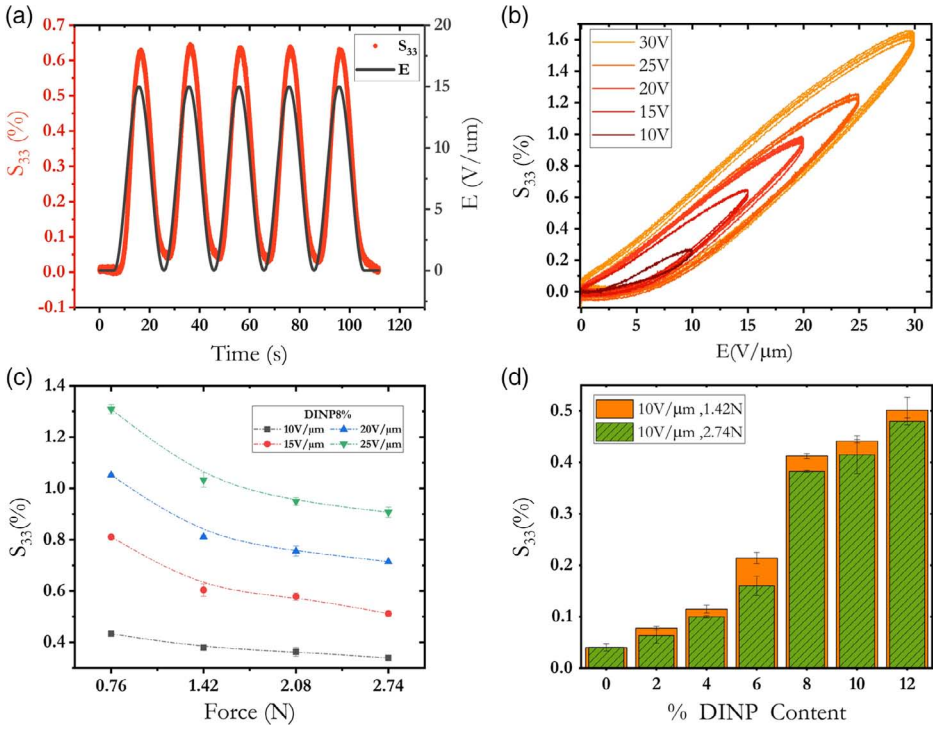


**Figure 6.** Longitudinal strain response ($S_{33}$) of the modified terpolymer doped with 8% DINP at an applied electric field: a) Temporal evolution of $S_{33}$ of the 8% sample excited by a 50 mHz sinus electric field with 15 V μm$^{-1}$ amplitude at preload 1.42 N. b) $S_{33}$ versus different levels of input electric field. c) $S_{33}$ versus applied forces at different electric fields. d) $S_{33}$ at two different preloads at $E = 10$ V μm$^{-1}$.

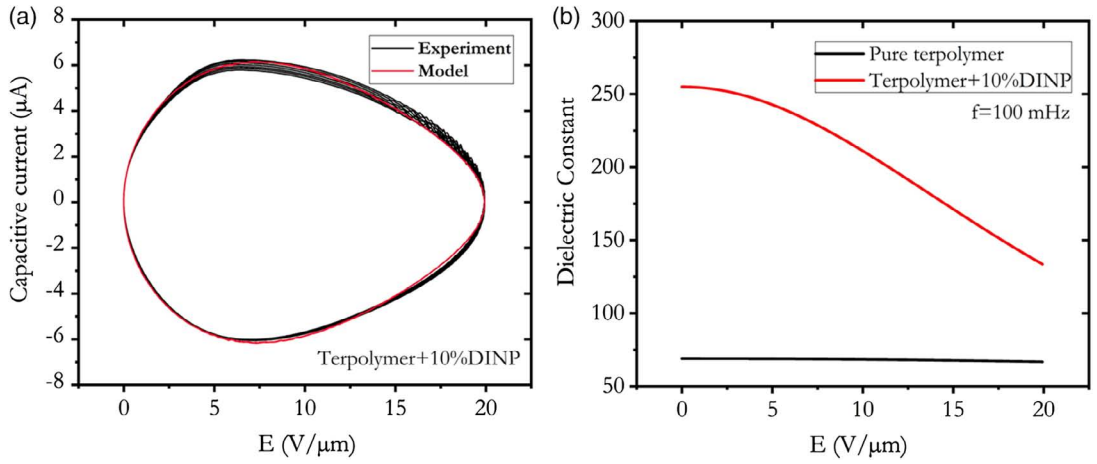


**Figure 7.** Evaluated electrical behavior of a plasticized 10%DINP terpolymer at an applied electric field $E$: a) the capacitive current after subtracting resistive current in response to the external applied electric filed and b) dielectric permittivity as a function of electric field.

results show that at a higher voltage range the dielectric constant drastically decreases as the dipole moments are not able to be further tilted and/or oriented at an electric field strength close to the saturated polarization of the material.

We observed that the current behavior of the plasticized terpolymer at a applied high electric field ($E \geq 10$V μm$^{-1}$) is unconventional with respect to pure terpolymer and other electrostrictive polymers.[34,40] According to empirical modeling, an estimated permittivity from Equation (4) using experimental current allows to evaluate the electromechanical response of the plasticized terpolymer at a high applied voltage. Instead of using the relative permittivity ($\varepsilon_r$) in Equation (1) and (2), the strain response ($S_{(E \gg E_0)}$) at a high input voltage can be inferred from the relative permittivity ($\varepsilon'_{(E)}$) as the following

$$S_{(E \gg E_0)} = \frac{\varepsilon_0 \varepsilon'_{(E)}}{Y} E^2 \tag{5}$$

In the end, such a trade-off among electromechanical coupling, dielectric breakdown strength, mechanical property

(Figure 6), and optimizing the dielectric permittivity as a function of the electric field (Figure 7) dictates the optimized material—the terpolymer filled with 8% or 10% of plasticizer—to be used as a force actuator for our Live Mirror development.

The main goal here is develop a multilayer topology to achieve extremely high permittivity while maintaining low losses. Preliminary consideration is that the permittivity is linearly increased in terms of the layers number. Based on the electric connection of each single film, the multilayer film was modeled as a structure of parallel capacitors and its resulting capacitance $C$ is

$$C = \sum_{k=1}^{n} C_k \Rightarrow C = nC_0 \tag{6}$$

where $C_k$ is the capacitance of the layer $k$ and $n$ is the number of layers, assuming that the capacitance of the $n$ layer is the same as $C_0$. As shown in **Figure 8**, the total longitudinal strain ($S_{total}$) of the pure and the plasticized (10% DINP) terpolymers for $n = 0$–6 layers was evaluated considering that $S_{total} \Rightarrow nS_{measured}$. The actuator capability of the doped terpolymer with a multilayered design showed an improved strain response when stimulated by a low input electric field ($E$). In particular, the quasistatic strain for the plasticized six-layer film at $E = 20\,\mathrm{V\,\mu m^{-1}}$ is almost an order of magnitude compared with the pure six-layer film (Figure 8a). Using the concept of the actuator's displacement prediction (Figure 2) as a function of external load (from 0.8 to 4.6 N), the strain response behavior is shown in Figure 8b. Experimental results demonstrated that the longitudinal strain gradually decreased versus the applied force, and the highest strain has been recorded for the plasticized six-layer film.

**Figure 9**a shows the image of the multilayer structure which consists of actuator layers with their top and bottom gold electrodes and adhesive layers including the electrical connection (aluminum foils) between actuator layers. The strain achievement of eight samples of the plasticized terpolymer film versus the layer number is shown in Figure 9b, at an alternative electric field of $10\,\mathrm{V\,\mu m^{-1}}$ (50 mHz frequency) and external load of 142 g or 458 g. The result showed that the linear relationship between the longitudinal strain and the number of layers ($S_{Total(n=1)} = 0.4\% \rightarrow S_{Total(n=8)} = 2.7\%$) is in good agreement with the model of Equation (1) and (2).

The results earlier confirm that the multilayer plasticized (10% DINP) EAP's actuator delivers an optimum actuation

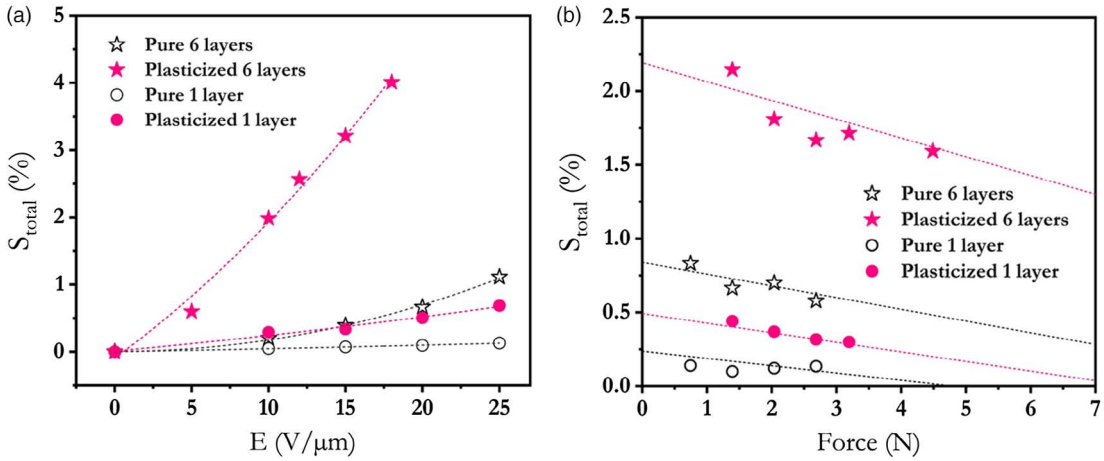


**Figure 8.** Total longitudinal strain ($S_{total}$) of the pure and the modified 10% DINP terpolymers for the single-layer and six-layer stack: a) $S_{total}$ versus electric field ($E$) under free force. b) $S_{total}$ versus force at $E = 10\,\mathrm{V\,\mu m^{-1}}$.

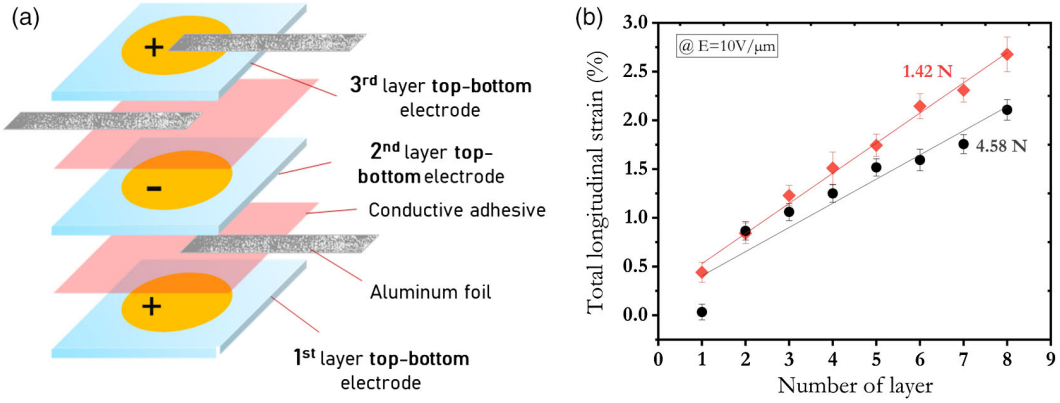


**Figure 9.** a) The schematic of the multilayer structure and b) total longitudinal strain ($S_{Total}$) versus number of layers ($n = 1$–8) for plasticized (10%DINP) terpolymers at applied external loads of 1.42 and 4.58 N.

performance at a low applied electric field ($E$) and a significant external load condition. Such a large strain is compliant with the Live Mirror force actuator development—seeking few microns of deformation at $E = 10$–$20\ \mathrm{V\ \mu m}$ and an external load of 1 N.

As a validation for the EAP's multilayer stack actuators, **Figure 10** shows a proof-of-concept prototype (concept based on Figure 1b) consisting of four identical eight-layer plasticized (10% DINP) actuators sandwiched between two flat 3 mm = thick pieces of glass—control $S_c$ and reaction $S_r$ surfaces. Each actuator was separately connected through a silver adhesive electrical path, what is possible to apply input voltage independently or simultaneously.

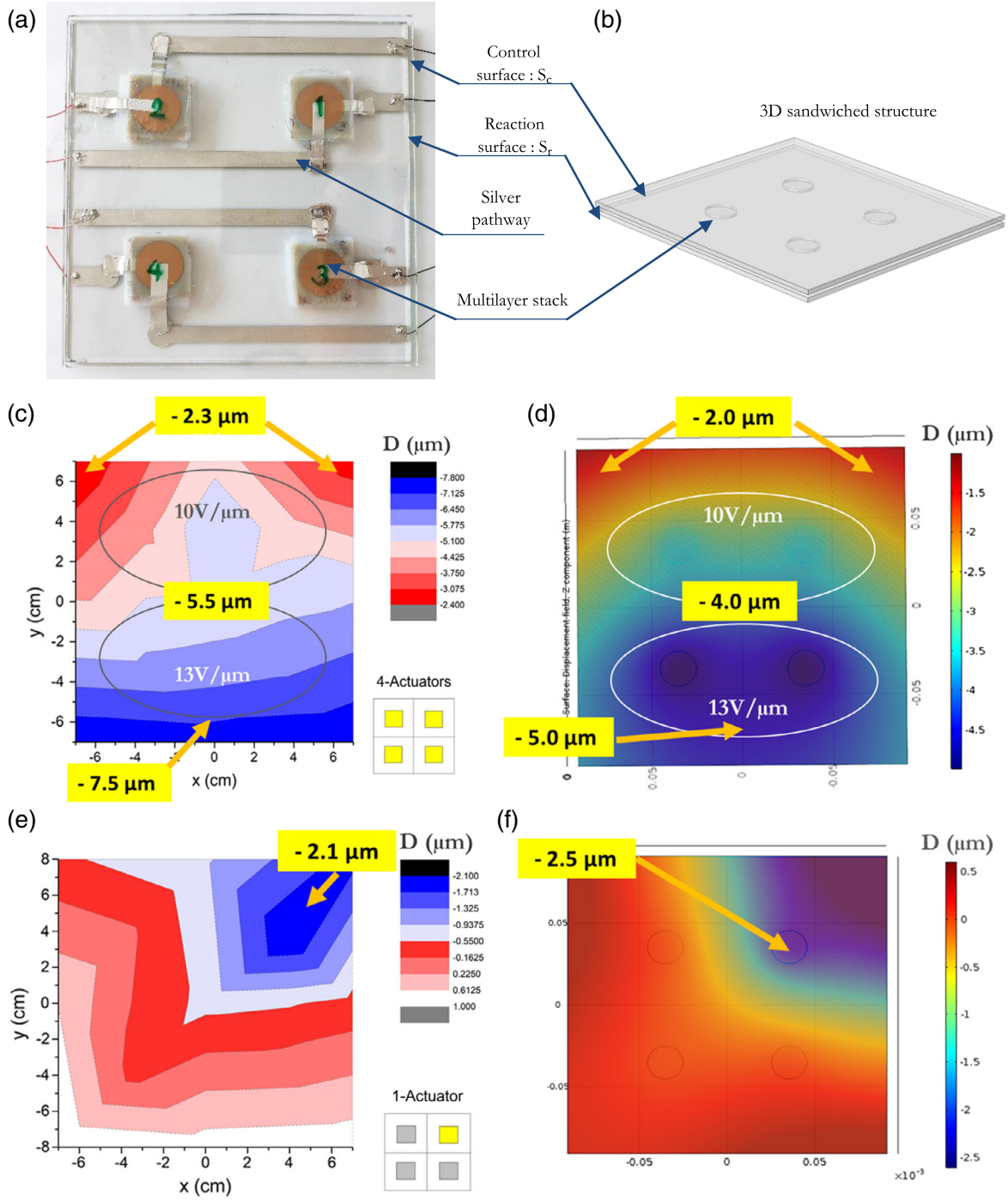


**Figure 10.** a) Sandwiched glasses with four stacks of actuators in square distribution and b) as modeled via COMSOL. The strain mapping results for the control surface ($S_c$) laser interferometrically measured are c) four actuators "in" at $E_{12} = 10\ \mathrm{V\ \mu m^{-1}}$ for actuators #1 and #2 and $E_{34} = 13\ \mathrm{V\ \mu m^{-1}}$ for actuators #3 and #4; e) $E_1 = 10\ \mathrm{V\ \mu m^{-1}}$ for actuator #1 "in" and $E_{234} = 0\ \mathrm{V\ \mu m^{-1}}$ actuators #s2, 3, and 4 "off". d,f) show the modelization and simulations results respectively for (c) and (e) configurations.

Deformation mapping on the control surface ($S_c$) was measured through laser interferometrics. Figure 10c shows the $S_c$ deformation map driven by four active actuators at different levels of input electric field, i.e. $E_{12} = 10\,\mathrm{V\,\mu m^{-1}}$ for actuators #1 and #2 and $E_{34} = 13\,\mathrm{V\,\mu m^{-1}}$ for actuators #3 and #4. As expected, the longitudinal strain response ($D$) increases as a function of the applied voltage, leading to a higher deformation in areas of actuators #3 and #4 with respect to area of the other samples; Figure 10d shows the same 3D model simulated by COMSOL Multiphysics code which confirms deformation in (c). Figure 10e shows the possibility to individually control actuators, i.e., an $E_1 = 10\,\mathrm{V\,\mu m^{-1}}$ on actuator #1, and it is confirmed by simulation in Figure 10f. In real life such a procedure provides a positive degree of freedom to control locally the optical surface. When experimental results ($D = 2.1$ μm) in Figure 10c,e are compared with the simulated ones ($D = 2.5$ μm) in Figure 10d,f, the slight difference is due the fact that the multilayer stack actuator contains a soft conductive adhesive transfer tape, which was neglected in the model simulations.

Subsequently, such architecture and the confirmed results by simulations significantly enhance the active surface spatial resolution, i.e., a precise and a local mirror control. As mentioned earlier, the EAP multilayer stack force actuator is intended to act/shape locally via longitudinal strain, following possible local changes in the glass global shape referred to here as global shaping.

Multilayered EAPs' shear force actuator is intended to act/shape via shear force (transversal strain) in reaction to possible glass surface shape deformations sensed by the sensor as local curvatures. Such actuation acts as local prepolishing, i.e., deforming/acting optimally on the optical shape of surface, and it is referred to here as electrical polishing.

A simplified shear architecture for a single-layer terpolymer and a glass flat surface is shown in **Figure 11**a, when no electric field is applied, e.g., no expansion stress is transferred to the control optical surface ($S_c$). When an electrical field is applied consequently, the EAP produces a transversal strain, transferring an expansion stress to the control optical surface, as shown Figure 11b. To improve the transversal strain $S$, a single EAP layer would be transformed in a multilayer (Seg1 + Seg2 + Seg3), producing $S_1 + S_2 + S_3$, where $S_1 < S_2 < S_3$ in the case as shown in Figure 11c. Seeking to accomplish the maximum deformation of the control optical surface produced by single-layer shear actuator, one would optimize the total (in our case Seg1 + Seg2 + Seg3) single-layer thickness $S_T$. Experimental results (**Figure 12**) show that the maximum displacement of the slumped glass tends to be saturated when the total thickness $S_T$ of the actuator reaches 1 mm, e.g., five layers of terpolymer (10%DINP) of 200 μm thickness for each single layer.

A multilayer EAP proof of concept was developed—a single 2 mm-thick glass surface $S_c$ with an integrated 8%DINP terpolymer with a 4 cm-diameter circular actuator (**Figure 13**a)—to operate in the shear mode. To characterize the shear force generated by transversal strain, deformation measurements $D_z$ of the control glass surface were assessed via a laser interferometer. Experimental results in Figure 13b,c show the control optical surface deformation $D_z$ respectively produced by the one-layer and the five-layer terpolymer at an electric field $E$ from 0 to 18 $\mathrm{V\,\mu m^{-1}}$ applied in the direction of thickness. The results show that the control optical surface significantly slumped down as it was induced by a transversal strain via external electric field $E$. The shear improvement measured by $D_z$ was 3× larger for the five-layers 8%DINP compared with the single-layer one.

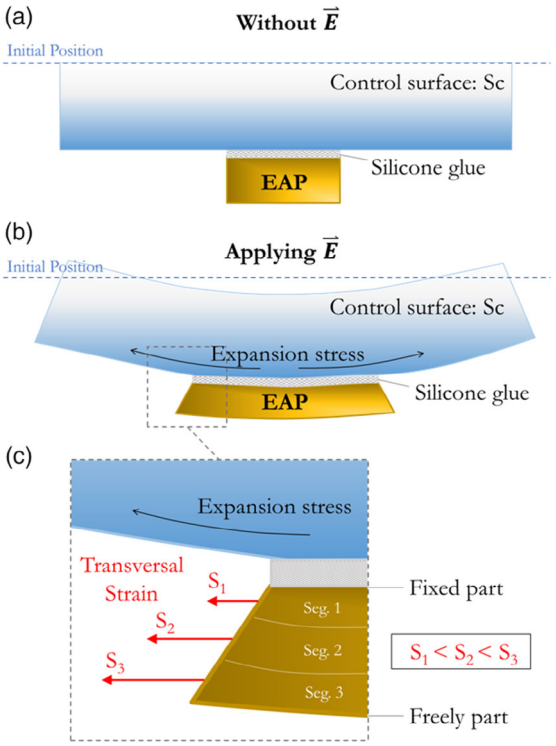


**Figure 11.** Shear actuator prototype illustration depicting the cross section of the sample: a) without electric field and b) at an applied electric field, the control surface ($S_c$) slumped down by the expansion stress from total EAP transversal strain.

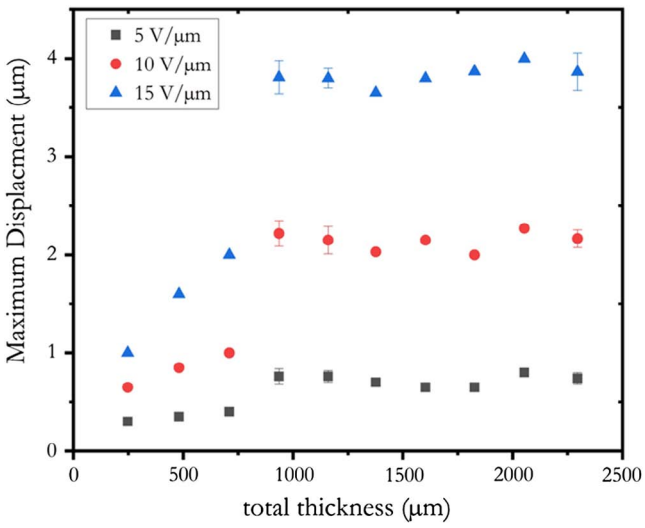


**Figure 12.** The maximum displacement at the center of the shear glass sample versus total thickness of actuator (summing up layer by layer) at three different levels of applied electric fields.

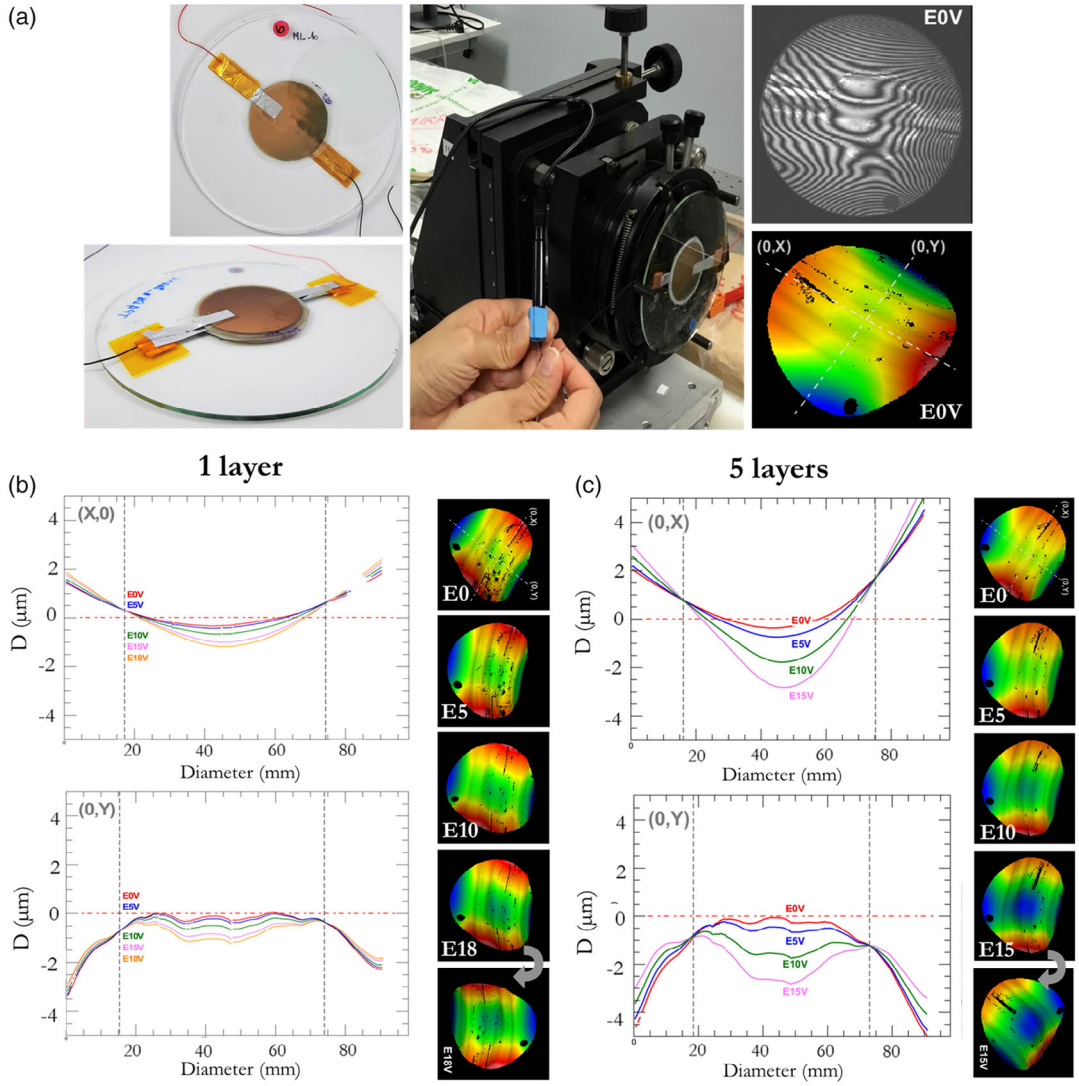


**Figure 13.** a) A multilayer EAP shear actuator proof of concept: a single 2 mm-thick glass optical surface $S_c$ with an integrated 8%DINP terpolymer with a 4 cm-diameter circular actuator. b,c) show 3D intensity plots on the (0,X) and (0,Y) orthogonal sections for the control optical surface deformation $D_z$ respectively produced by the one-layer terpolymer and the five-layer terpolymer at an electric field $E$ from 0 to 18V µm$^{-1}$ applied in the thickness direction.

These preliminary results for the proof-of-concept shear actuator confirm the feasibility of a mode of force actuators acting/deforming via shear force (transversal strain) locally on a control optical surface, i.e., deforming optimally on the optical shape of surface electrical polishing.

A novel hybrid active shape control design based on a doped/plasticized terpolymer has been demonstrated. The proposed architectures in the multilayer stack force actuators for global shaping and for shear "electrical polishing" modes generate respectively large longitudinal and transversal strains at moderate electric fields and for realistic load conditions. Experimental results showed the great potential for thin glass shape correction with EAP force actuators. This is useful for shape control of reflective optical surfaces. Achieving active shape control with many degree-of-freedom EAP force actuators will use additive 3D printing-based technology, as demonstrated here. Such a controlled EAP glass sandwich system creates a hybrid metamaterial with good effective stiffness-to-density ratio properties. The development of 3D-printable actuators for force and sensing will allow scalable systems with hundreds of actuators and high precision that allows deformation resolutions in the nanometer range with maximum deformations of several micrometers—a main goal for the Live Mirror project.

## Acknowledgements

This project was sponsored by The French National Research Agency (ANR): project #ANR-18-CE42-0007-01 (Live Mirror project, PIs G.M. and J-F.C.). K.T. acknowledges support from DPST Thai scholarship jointly administered by the Ministry of Education and the Institute for the Promotion of Teaching science and Technology Thailand and Franco–Thai scholarship 2016 from Campus France. The authors thank

 

INSA-Lyon for supporting the grant given to Professor J.K. and Carnot Institute for their financial support. The authors also thank Assistant Professor Chatchai Putson for assistance with Thai internships (S.C. and W.K.).

## Conflict of Interest

The authors declare no conflict of interest.

## Keywords

active optics, actuator applications, astronomy and optical communication applications, deformable mirrors, modified electroactive polymers, multilayer actuators, plasticized terpolymers

Received: December 17, 2019
Revised: January 30, 2020
Published online: February 28, 2020

[1] C. Ning, Z. Zhou, G. Tan, Y. Zhu, C. Mao, *Prog. Polym. Sci.* **2018**, *81*, 144.
[2] Y. Bar-cohen, S. Leary, *Smart Struct. Mater. Mater.* **2000**, *3987*, 12.
[3] Q. Xiao, X. Wang, W. Li, Z. Li, T. Zhang, H. Zhang, *J. Memb. Sci.* **2009**, *334*, 117.
[4] E. Mooney, J. N. Mackle, D. J. P. Blond, E. O'Cearbhaill, G. Shaw, W. J. Blau, F. P. Barry, V. Barron, J. M. Murphy, *Biomaterials* **2012**, *33*, 6132.
[5] F. Ganet, M. Q. Le, J. F. Capsal, J. F. Gérard, S. Pruvost, J. Duchet-Rumeau, S. Livi, P. Lermusiaux, A. Millon, P. J. Cottinet, *Sens. Actuators B Chem.* **2015**, *220*, 1120.
[6] S. Z. Guo, K. Qiu, F. Meng, S. H. Park, M. C. McAlpine, *Adv. Mater.* **2017**, *29*, 1.
[7] T. P. D. Rajan, J. M. Gladis, *Biomed. Appl. Polym. Mater. Compos.* **2016**, 125.
[8] M. Shahinpoor, *Electrochim. Acta* **2003**, *48*, 2343.
[9] Y. Wang, Y. Hou, Y. Deng, *Compos. Sci. Technol.* **2017**, *145*, 71.
[10] M. Dorfmeister, B. Kössl, M. Schneider, U. Schmid, *Proceedings* **2019**, 2.
[11] F. Xia, Z. Cheng, H. Xu, H. Li, Q. Zhang, G. J. Kavarnos, R. Y. Ting, G. Abdul-Sedat, K. D. Belfield, *Adv. Mater.* **2002**, *14*, 1574.
[12] X. Yin, J. F. Capsal, D. Guyomar, *Appl. Phys. Lett.* **2014**, *104*, 2012.
[13] J. F. Capsal, J. Galineau, M. Q. Le, F. Domingues Dos Santos, P. J. Cottinet, *J. Polym. Sci. B Polym. Phys.* **2015**, *53*, 1368.
[14] T. Mirfakhrai, J. D. W. Madden, R. H. Baughman, *Mater. Today* **2007**, *10*, 30.
[15] S. Rudykh, K. Bhattacharya, G. Debotton, *Int. J. Non. Linear. Mech.* **2012**, *47*, 206.
[16] M. Q. Le, J. F. Capsal, J. Galineau, F. Ganet, X. Yin, M. D. Yang, J. F. Chateaux, L. Renaud, C. Malhaire, P. J. Cottinet, R. Liang, *Sci. Rep.* **2015**, *5*, 1.
[17] F. Ganet, M. Q. Le, J. F. Capsal, P. Lermusiaux, L. Petit, A. Millon, P. J. Cottinet, *Sci. Rep.* **2015**, *5*, 1.
[18] B. H. Chen, L. Wu, M. C. Chure, Y. C. Chen, *Proc. 2010 Symp. Piezoelectricity, Acoust. Waves Device Appl. SPAWDA10*, IEEE, Xiamen, Fujian, China **2010**, p. 310.
[19] L. Ruan, D. Zhang, J. Tong, J. Kang, Y. Chang, L. Zhou, G. Qin, X. Zhang, *Ferroelectr. Their Appl.* **2018**, https://doi.org/10.5772/intechopen.77167.
[20] G. Miron, B. Bédard, J.-S. Plante, *Actuators* **2018**, *7*, 40.
[21] S. T. Choi, J. O. Kwon, F. Bauer, *Sens. Actuators A Phys.* **2013**, *203*, 282.
[22] S. T. Choi, J. O. Kwon, W. Kim, F. Bauer, *Proc. Int. Symp. Electrets*, IEEE, Montpellier, France **2011**, 61.
[23] J. W. Hardy, *Proc. IEEE*, IEEE, Lexington, MA **1977**, 651.
[24] V. Costes, L. Perret, D. Laubier, J. M. Delvit, *Int. Soc. Opt. Photonics* **2017**, *10562*, 1.
[25] N. Devaney, K. Fiona, V. G. Alexander, G. Matthias, R. Claudia, *Appl. Opt.* **2018**, *57*, E138.
[26] G. Moretto, J. R. Kuhn, J. F. Capsal, D. Audigier, K. Thetpraphi, M. Langlois, M. Tallon, M. Gedig, S. V. Berdyugina, D. Halliday, *Proc. SPIE. Int. Soc. Opt. Eng.*, Optical Society of America, Orlando, FL **2018**, p. 10700, https://doi.org/10.1117/12.2312599.
[27] J. R. Kuhn, S. V Berdyugina, M. Gedig, M. Langlois, G. Moretto, K. Thetpraphi, *Soc. Photo-Optical Instrum. Eng. Conf. Ser.* **2018**, 10700.
[28] G. Moretto, J. Kuhn, J.-F. Capsal, D. Audigier, K. Thetpraphi, M. Langlois, M. Gedig, S. V. Berdyugina, D. Halliday, *Hybrid Dynamic Structures for Optical-Quality Surfaces Shape Control: Live-Mirror*, Vol. *10926*, SPIE, San Francisco, CA **2019**.
[29] K. Thetpraphi, M. Q. Le, A. Houachtia, P. Cottinet, L. Petit, D. Audigier, J. Kuhn, G. Moretto, J. Capsal, *Adv. Opt. Mater.* **2019**, *1900210*, 1900210.
[30] J. Pritchard, C. R. Bowen, F. Lowrie, *Br. Ceram. Trans.* **2001**, *100*, 265.
[31] Y. Song, S. Qin, J. Gerringer, J. Grunlan, *Soft Matter* **2019**, *15*, 2311.
[32] L. Wang, H. Luo, X. Zhou, X. Yuan, K. Zhou, D. Zhang, *Compos. Part A* **2019**, *117*, 369.
[33] F. Li, L. Jin, Z. Xu, S. Zhang, *Appl. Phys. Rev.* **2014**, *1*, https://doi.org/10.1063/1.4861260.
[34] N. Della Schiava, M. Q. Le, J. Galineau, F. Domingues Dos Santos, P. J. Cottinet, J. F. Capsal, *J. Polym. Sci. Part B Polym. Phys.* **2017**, *55*, 355.
[35] N. Della Schiava, K. Thetpraphi, M. Q. Le, P. Lermusiaux, A. Millon, J. F. Capsal, P. J. Cottinet, *Polymers* **2018**, *10*, 1.
[36] J.-F. Capsal, M. Lallart, J. Galineau, P.-J. Cottinet, G. Sebald, D. Guyomar, *J. Phys. D. Appl. Phys.* **2012**, *45*, 205401.
[37] M. Rahman, C. S. Brazel, *Prog. Polym. Sci.* **2004**, *29*, 1223.
[38] L. Zhu, *J. Phys. Chem. Lett.* **2014**.
[39] J. F. Capsal, J. Galineau, M. Lallart, P. J. Cottinet, D. Guyomar, *Sens. Actuators, A Phys.* **2014**, *207*, 25.
[40] F. Pedroli, A. Marrani, M. Q. Le, O. Sanseau, P. J. Cottinet, J. F. Capsal, *RSC Adv.* **2019**, *9*, 12823.

 